ELSEVIER

Coordination Chemistry Reviews
216–217 (2001) 3–30

COORDINATION CHEMISTRY REVIEWS

www.elsevier.com/locate/ccr

Doubly pyridazine-bridged macrocyclic complexes of copper in +1, +2 and mixed valent oxidation states

Sally Brooker [a,*], Tony C. Davidson [a], Sarah J. Hay [a], Robert J. Kelly [a], Dietmar K. Kennepohl [a,b], Paul G. Plieger [a], Boujemaa Moubaraki [c], Keith S. Murray [c], Eckhard Bill [d], Eberhard Bothe [d]

[a] *Department of Chemistry, University of Otago, PO Box 56, Dunedin, New Zealand*
[b] *Centre for Science, Athabasca University, 1 University Drive, Athabasca, Alberta, Canada T9S 3A3*
[c] *Department of Chemistry, Monash University, Clayton, Victoria 3168, Australia*
[d] *Max-Planck-Institut für Strahlenchemie, Stiftstrasse 34-36, D-45470 Mülheim an der Ruhr, Germany*

Received 8 August 2000; accepted 30 October 2000

Contents

* Corresponding author. Tel.: +64-3-4797919; fax: +64-3-4797906.
E-mail address: sbrooker@alkali.otago.ac.nz (S. Brooker).

PII: S0010-8545(00)00399-4

Abstract

Transmetallation of the dilead(II) complex $[Pb_2(L1')](ClO_4)_4$ [L1′ is the (4 + 4) Schiff-base macrocycle derived from 3,6-diformylpyridazine and 1,3-diaminopropane] with copper(II) perchlorate results in the formation of a dicopper(II) complex of the (2 + 2) Schiff-base macrocycle L1, $Cu^{II}_2(L1)(ClO_4)_4$ (**1**). Copper(II) is unable to template the formation of **1** from the organic precursors. A series of six dicopper(II) complexes of L1 has been prepared from **1**, including: $[Cu^{II}_2(L1)X_2](ClO_4)_2$ (where $X = Cl^-$ **2**, Br^- **3**, I^- **4**, NCS^- **5**), $Cu^{II}_2(L1)(H_2O)_2(NO_3)_2(ClO_4)_2$ (**6**) and $Cu^{II}_2(L1)(H_2O)_2(ClO_4)_4$ (**7**). Three of these dicopper(II) complexes, **1**$^{\bullet}$2MeCN, **2**$^{\bullet}H_2O$ and **7**, have been characterised by X-ray crystallography. In all three cases the (2 + 2) macrocycle provides a double pyridazine bridge between the two copper(II) ions. Magnetic studies show that the double pyridazine bridge mediates strong antiferromagnetic exchange between the copper(II) ions in all of these complexes ($-2J =$ 412 to 532 cm^{-1}). Electrochemical and spectroelectrochemical studies reveal that reduction of the dicopper(II) complexes occurs in two one electron steps, via stable mixed valent intermediates ($K_c = 3.8 \times 10^5$ to 8.6×10^6 in acetonitrile, MeCN), in marked contrast to all previously studied pyridazine-bridged dicopper complexes. The thiocyanate salt of the mixed valent complex, $[Cu^{II}Cu^{I}(L1)(NCS)_4Cu^{I}]$MeCN (**9**), has been isolated, by transmetallation of $[Pb_2(L1')](ClO_4)_4$ with copper(I) followed by the addition of NaNCS, and structurally characterised. Finally, the previously reported grid complex, $[Cu^{I}_4(L1)_2](PF_6)_4$ (**10**) [formed by templating L1 formation on copper(I) ions], is shown by NMR spectroscopy to exist in equilibrium with another species, presumed to be a dicopper(I) complex, $[Cu^{I}_2(L1)(MeCN)_2](PF_6)_2$ (**11**), in acetonitrile solution. In support of this assignment, the structure of the dicopper(I) complex, $[Cu^{I}_2(L1)(PPh_3)_2](PF_6)_2$ (**12**), isolated from reaction of **10** with two equivalents of PPh_3, is reported.

Keywords: Macrocycle; Copper; Mixed-valent; Pyridazine; X-ray crystal structure; Electrochemistry

1. Introduction

Much of the research into the coordination chemistry of polydentate ligands containing either pyridazine or phthalazine has focused on the copper(II) complexes of these ligands [1–4]. The diazine bridge between the coordinated copper(II) centres has been shown to mediate significant antiferromagnetic exchange, and the factors affecting the nature of this exchange have been thoroughly examined. Electrochemical investigations of these dicopper(II) complexes have shown that they generally undergo one two-electron reduction at a positive potential [3]. Hence mixed valent copper(II)copper(I) complexes were unknown until very recently [5]. Isolation of the related dicopper(I) complexes has been achieved in only a few cases [3], but some polymetallic copper(I) grid complexes have also been studied [5,6].

Of the many pyridazine-containing ligands studied, very few have been macrocyclic [5,7–10], and prior to our work [5,7–9] none had contained a pyridazine bridge between the incorporated metal ions [10]. Recently we reported the successful introduction of the new head unit 3,6-diformylpyridazine in to Schiff base macrocyclic chemistry [7] and subsequently we communicated the isolation of the first pyridazine-bridged macrocyclic dicopper(II) complex, $Cu_2(L1)(ClO_4)_4$ (**1**) (Fig. 1) [8]. Herein we detail the synthesis, structure, magnetic, electrochemical and spectroelectrochemical properties of a series of pyridazine-bridged copper complexes of the macrocyclic Schiff base ligand L1, and draw comparisons with complexes of related acyclic pyridazine ligands [2–4] and symmetrical phenol macrocycles (e.g. L2, Fig. 1) [11–13].

2. Results and discussion

2.1. Synthesis

Transmetallation of an acetonitrile solution of $[Pb_2(L1')](ClO_4)_4$ (where L1′ is the $4+4$ macrocycle version of the $2+2$ macrocycle L1) with four equivalents of

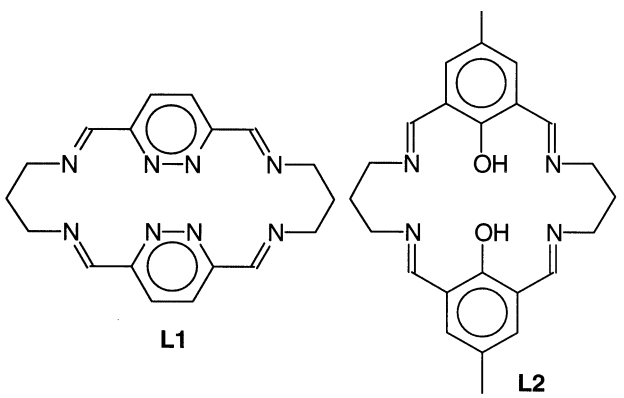

Fig. 1. Ligands L1 (used in this study) and L2.

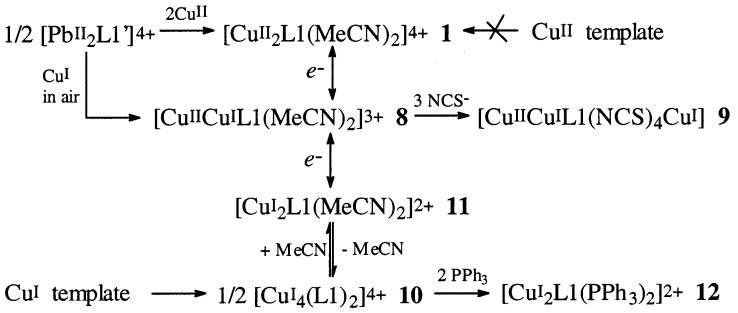

Scheme 1.

$Cu(ClO_4)_2.6H_2O$ yields $Cu^{II}_2(L1)(ClO_4)_4$ (**1**) (Scheme 1) [7,8]. Copper(II) is unable to act as a template for the direct preparation of **1** from 3,6-diformylpyridazine and 1,3-diaminopropane: a brown oil forms on diffusion of diethyl ether into the acetonitrile reaction solution. Compounds **2**–**6** were subsequently prepared from **1**, in acetonitrile, by replacement of two of the perchlorate ions with the different counter ions, Cl^-, Br^-, I^-, NCS^- and NO_3^-, respectively. Compound **7** was obtained from an unsuccessful attempt to introduce an exogenous pyridazine bridge. The insolubility of compounds **2**, **3** and **5** in acetonitrile allowed the analytically clean products to be filtered directly from the reaction mixture, whereas **4** was isolated by diethyl ether diffusion into the reaction solution and compounds **6** and **7** were isolated by slow evaporation of the reaction solutions. Difficulty was experienced in reproducing the accidental preparation of **7**.

Further to the previously reported synthesis of the mixed valent dicopper complex $[Cu^{II}Cu^{I}(L1)(MeCN)_2](ClO_4)_2(PF_6)$ (**8**) (Scheme 1) [5], it should be noted that on leaving a transmetallation solution of $[Pb_2(L1')](ClO_4)_4$ and four equivalents of copper(I) in air for 4 weeks the UV–vis spectrum of the resulting solution remains consistent with formation of the mixed valent complex **8** (Fig. 11). Another mixed valent complex, $[Cu^{II}Cu^{I}(L1)(NCS)_4Cu^{I}]MeCN$ (**9**), has also been isolated. Crystals of **9** were unexpectedly obtained by adding three equivalents of NaSCN to **8** in an attempt to produce the thiocyanate analogue of **8** (Scheme 1). A subsequent deliberate synthesis of the tricopper mixed valent complex **9**, from **8** with stoichiometric amounts of Cu^{I} and NaSCN, has improved the yield.

The template reaction of 3,6-diformylpyridazine and 1,3-diaminopropane on copper(I) ions results in the formation of the previously reported, air stable, grid complex, $[Cu^{I}_4(L1)_2](PF_6)_4$ (**10**) [5]. The dicopper(I) complex, $[Cu^{I}_2(L1)(PPh_3)_2](PF_6)_2$ (**12**), is obtained from an acetonitrile solution of **10** by adding two equivalents of PPh_3 under nitrogen, and then diffusing the reaction solution with diethyl ether in air.

IR analysis of new compounds **1**–**7**, **9** and **12** yielded, as expected, very similar results. Perchlorate or thiocyanate or hexafluorophosphate bands (for **1**–**7** ca. 1080 and 625 cm^{-1}, for **9** 2080 cm^{-1}, for **12** 842 and 558 cm^{-1}), an imine peak (ca.

1635–1650 cm^{-1}), and two peaks characteristic of the pyridazine rings (ca. 1580 and 1550 cm^{-1}) were seen in all of the IR spectra. A similar fragmentation pattern was seen in the FAB mass spectra of all of the dicopper(II) compounds **1**–**7**: three signals, with m/z 573, 474, and 411, corresponding to fragments $[Cu_2(L1)(ClO_4)]^+$, $[Cu_2(L1)]^+$ and $[Cu(L1)]^+$, respectively, are common to all of the spectra. Fragments of the general formulae $[Cu(L1)(ClO_4)X]^+$ and $[Cu(L1)X]^+$, where $X = Cl^-$, Br^-, I^-, NCS^- or NO_3^-, are also observed in the spectra of **2** to **6**, respectively. The FAB mass spectrum of complex **12** had a clear signal corresponding to $[Cu_2(L1)(PPh_3)(PF_6)]^+$; fragments of this species were observed at lower m/z. No evidence for the presence of L1′ [the (4 + 4) version of L1] complexes was observed in any case.

2.2. Description of the structures

The structures of $Cu_2^{II}(L1)(ClO_4)_4$ (**1**), as the bis-acetonitrile complex $[Cu_2^{II}(L1)(MeCN)_2](ClO_4)_4$, $[Cu^{II}Cu^{I}(L1)(MeCN)_2](ClO_4)_2(PF_6)$ (**8**) and $[Cu_4^{I}(L1)_2](PF_6)_4$ (**10**) have been communicated previously [5,8]. The structures of complexes **2**•H_2O, **7**, **9** and **12** are shown in Figs. 2–6, respectively. Selected interatomic distances and angles are given in the figure captions.

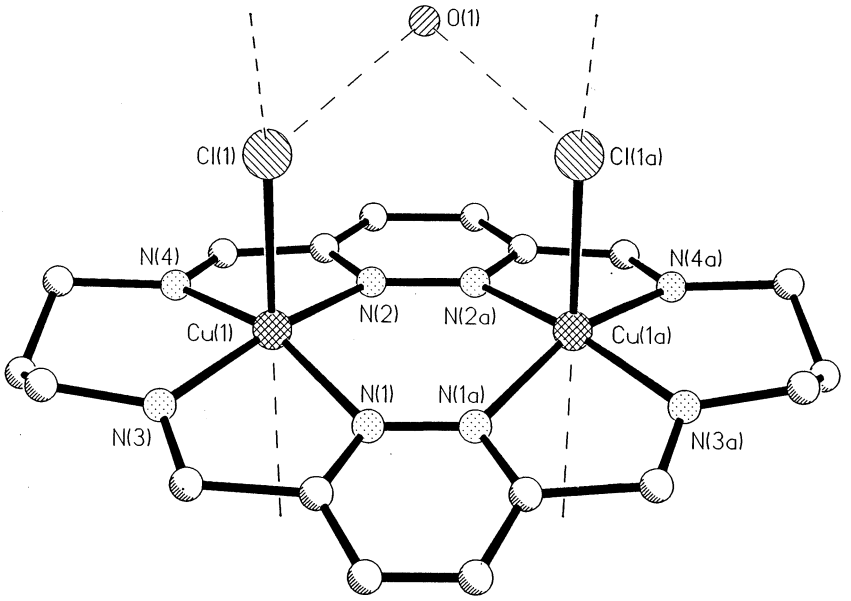

Fig. 2. Perspective view of $[Cu_2(L1)Cl_2(H_2O)](ClO_4)_2$, **2**·$(H_2O)$. The two perchlorate ions and the hydrogen atoms have been omitted for clarity.

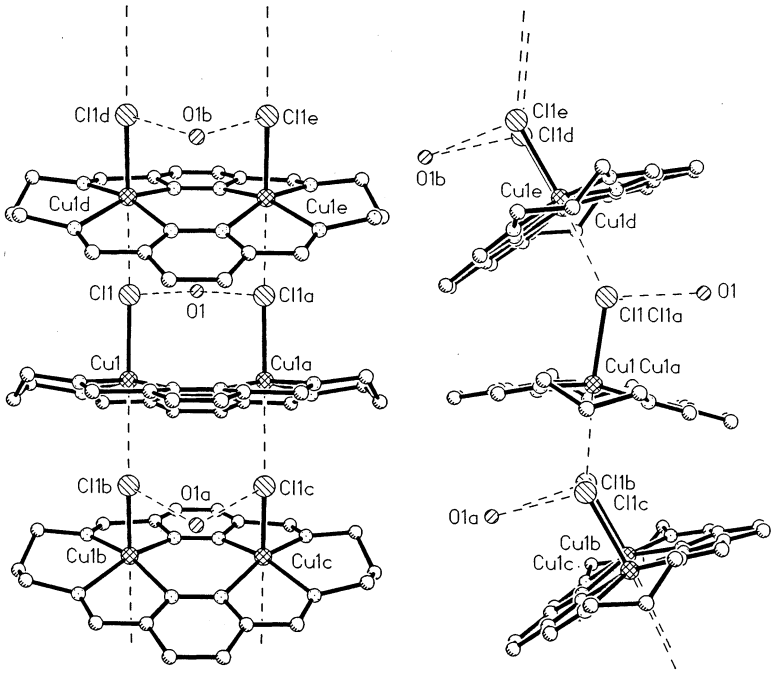

Fig. 3. Perspective diagrams showing the stacking of the $[Cu_2(L1)Cl_2(H_2O)]^{2+}$ units via close contacts between adjacent copper and chlorine atoms. The hydrogen atoms and perchlorate ions have been omitted for clarity.

Single crystals of $[Cu^{II}_2(L1)Cl_2(H_2O)](ClO_4)_2$, **2**•$H_2O$, were grown by the diffusion of diethyl ether into a dimethylformamide solution. The crystals were only just of adequate quality for study by X-ray diffraction but did allow the structure to be determined (Fig. 2 and Fig. 3). The copper(II) atoms are in crystallographically identical binding environments as they are related by a mirror plane which is located between them perpendicular to the plane of the macrocycle and bisecting the pyridazine rings (Fig. 2). Each copper atom is bound by four nitrogen donors, which make up the basal plane, and an apically bonded chloride atom. The chloride atoms are bound on the same side of the macrocyclic ring (*cis*), and the copper atoms are drawn out of the basal planes towards these chloride atoms, similar to the copper atoms in **1** which are 0.317(2) Å out of plane towards the apical acetonitrile molecules. A weak interaction also exists between each copper atom and the chloride atom of a neighbouring molecule and this results in the $[Cu^{II}_2(L1)Cl_2(H_2O)]^{2+}$ cations stacking up in a ladder arrangement (Fig. 3).

Crystals of $[Cu^{II}_2(L1)(H_2O)_2](ClO_4)_4$ (**7**) were successfully grown by slow evaporation of an acetonitrile solution saturated with sodium perchlorate and the structure determined by X-ray crystallography (Fig. 4). The two halves of the molecule are related by a centre of inversion. Each copper atom has two pyridazine nitrogen donors and two imine nitrogen donors coordinated in the basal plane and a water

molecule coordinated to the apical site. The two copper atoms are displaced slightly out of the respective N_4 basal planes towards the apically bonded oxygen atoms of the water molecules [0.112(4) Å] (Fig. 4). The bound water molecules sit on opposite sides of the macrocyclic ring (*trans*) and are involved in hydrogen bonds to two of the perchlorate counter ions [O(1)..O(11) and O(1)..O(1b) distances of 2.808(11) and 3.105(16) Å, respectively]. There is also a long, weak interaction between the open face of each copper atom and an oxygen atom from one of the perchlorate molecules [Cu(1)..O(14a) 2.936(11) Å], similar to that seen in $[Cu_2^{II}(L1)(MeCN)_2](ClO_4)_4$. Other than the central carbon atoms of the alkyl lateral groups, the macrocycle itself is flat. This leads to a greater copper–copper separation in **7** [3.888(3) Å] than is observed in the slightly bowed $[Cu_2^{II}(L1)(MeCN)_2](ClO_4)_4$ [3.805(3) Å] complex [8].

Crystals of $[Cu^{II}Cu^{I}(L1)(NCS)_4Cu^{I}]MeCN$ (**9**), were obtained from the reaction solution on standing and the structure determined (Fig. 5). This revealed that the mixed valent macrocyclic complex had removed a copper atom from another

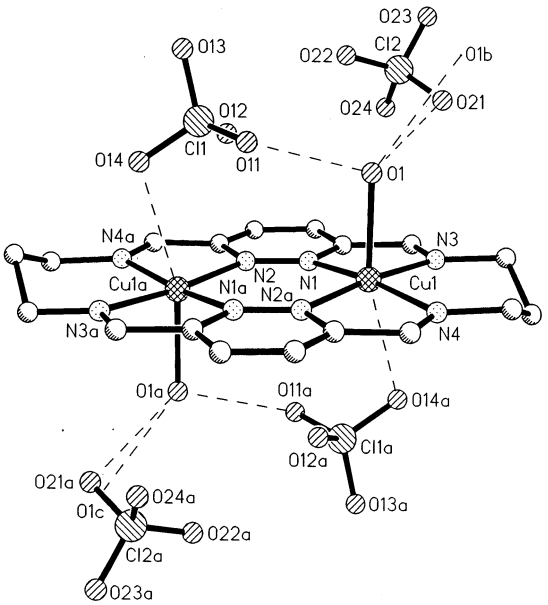

Fig. 4. Perspective diagram of $[Cu_2(L1)(H_2O)_2](ClO_4)_4$ (**7**) showing the hydrogen bonding interactions and the weak interactions between the copper ions and perchlorate oxygen atoms. The hydrogen atoms have been omitted for clarity. Selected interatomic distances (Å) and angles (°): Cu(1)–N(3) 1.989(8), Cu(1)–N(4) 1.998(8), Cu(1)–N(2a) 2.026(8), Cu(1)–N(1) 2.056(7), Cu(1)–O(1) 2.180(7), N(2)–Cu(1a) 2.026(8), Cu(1a)..O(14) 2.936(11), Cu(1)..Cu(1a) 3.888(3), N(3)–Cu(1)–N(4) 94.2(3), N(3)–Cu(1)–N(2a) 174.2(3), N(4)–Cu(1)–N(2a) 81.2(3), N(3)–Cu(1)–N(1) 81.8(3), N(4)–Cu(1)–N(1) 170.6(3), N(2a)–Cu(1)–N(1) 102.1(3), N(3)–Cu(1)–O(1) 90.3(3), N(4)–Cu(1)–O(1) 94.0(3), N(2a)–Cu(1)–O(1) 93.6(3), N(1)–Cu(1)–O(1) 94.6(3), N(2)–N(1)–Cu(1) 128.3(6), N(2)–C(2)–C(3) 121.9(9), N(2)–C(2)–C(11a) 113.4(9), C(5)–N(1)–Cu(1) 110.9(6), C(2)–N(2)–Cu(1a) 111.6(7), N(1)–N(2)–Cu(1a) 129.2(6).

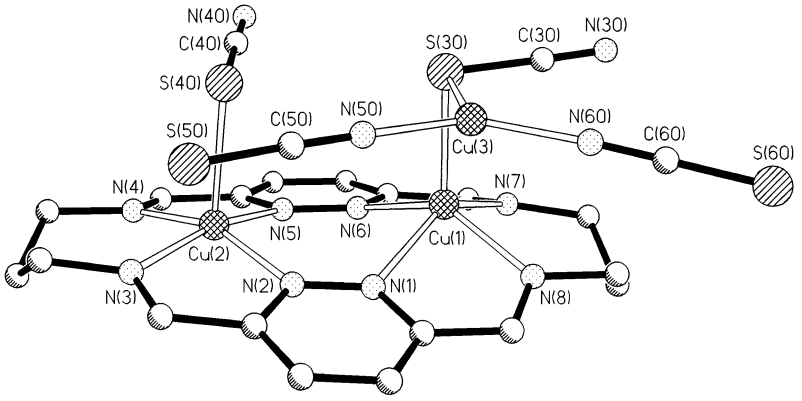

Fig. 5. Perspective view of $[Cu^{II}Cu^{I}(L1)(NCS)_4Cu^{I}]$ (**9**). Selected interatomic distances (Å) and angles (°): Cu(1)–N(8) 2.079(2), Cu(1)–N(7) 2.123(2); Cu(1)–N(6) 2.1572(18), Cu(1)–N(1) 2.1888(19), Cu(1)–S(30) 2.3023(8), Cu(2)–N(4) 2.0095(19), Cu(2)–N(3) 2.010(2), Cu(2)–N(2) 2.0367(18), Cu(2)–N(5) 2.0552(18), Cu(2)–S(40) 2.4740(9), Cu(3)–N(50) 1.895(2), Cu(3)–N(60) 1.899(2), Cu(3)–S(30) 2.3457(8), Cu(1)…Cu(2) 3.8986 (0.0009), Cu(1)… Cu(3) 3.2299 (0.0007), Cu(2)…Cu(3) 5.2112 (0.0010), N(8)–Cu(1)–N(7) 89.49(8), N(8)–Cu(1)–N(6) 141.95(7), N(7)–Cu(1)–N(6) 77.31(7), N(8)–Cu(1)–N(1) 76.90(7), N(7)–Cu(1)–N(1) 141.71(7), N(6)–Cu(1)–N(1) 91.60(7), N(8)–Cu(1)–S(30) 112.21(6), N(7)–Cu(1)–S(30) 106.39(6), N(6)–Cu(1)–S(30) 105.76(5), N(1)–Cu(1)–S(30) 111.90(5), N(4)–Cu(2)–N(3) 92.37(8), N(4)–Cu(2)–N(2) 159.24(8), N(3)–Cu(2)–N(2) 80.13(8), N(4)–Cu(2)–N(5) 80.30(8), N(3)–Cu(2)–N(5) 163.26(8), N(2)–Cu(2)–N(5) 101.50(7), N(4)–Cu(2)–S(40) 100.86(6), N(3)–Cu(2)–S(40) 98.37(6), N(2)–Cu(2)–S(40) 99.37(6), N(5)–Cu(2)–S(40) 97.79(5), N(50)–Cu(3)–N(60) 134.84(9), N(50)–Cu(3)–S(30) 110.60(7), N(60)–Cu(3)–S(30) 114.46(6), C(30)–S(30)–Cu(1) 92.55(8), C(30)–S(30)–Cu(3) 98.11(8), Cu(1)–S(30)–Cu(3) 88.03(2), C(40)–S(40)–Cu(2) 96.75(9), C(50)–N(50)–Cu(3) 176.5(2), C(60)–N(60)–Cu(3) 174.5(2).

macrocycle to form a tricopper complex. This additional copper atom, Cu(3), lies above the fairly flat macrocycle [the pyridazine ring planes intersect at 21.75(6)°] and is coordinated to three thiocyanate molecules, one of which provides an S-only bridge to Cu(1). The two copper ions held within the macrocycle are doubly bridged by pyridazine moieties. Both are five coordinate but there are differences in the geometries which indicate that the valences are localised (as for **8**, vide infra): Cu(1) is assigned to be in the $+1$ oxidation state [average Cu(1)–$N_{macro} = 2.137$ Å; Cu(1) is 0.6985 (10) Å out of the $(N_{macro})_4$ plane towards S(30)] whereas Cu(2) is assigned to be in the $+2$ oxidation state [average Cu(2)–$N_{macro} = 2.028$ Å; Cu(2) is 0.3198 (10) Å out of the $(N_{macro})_4$ plane towards S(40)].

Crystals of $[Cu^{I}_2(L1)(PPh_3)_2](PF_6)_2$ (**12**) were obtained from the acetonitrile reaction solution by diethyl ether diffusion and the structure determined by X-ray crystallography (Fig. 6). The two halves of the complex are related to each other by a centre of inversion. Each five coordinate copper atom has two pyridazine nitrogen donors and two imine nitrogen donors coordinated in the basal plane and a triphenylphosphine molecule coordinated to the apical site. Consistent with the $+1$ oxidation state the copper atoms are displaced 0.8223(11) Å out of their N_4 basal

planes towards the apically bonded phosphorous atoms of the triphenylphosphine molecules, and the average Cu(1)–N_{macro} distance [2.187(2) Å] is comparable to that observed for Cu(1) in **9**. The bulky triphenylphospine molecules sit on opposite sides of the macrocyclic ring (*trans*). As the copper(I) ions are therefore displaced in opposite directions relative to the macrocyclic ring, this complex has the largest copper–copper separation [4.4316(12) Å] observed for this macrocycle to date.

In complexes **1**, **7** and **9** the doubly pyridazine-bridged copper ions are separated by a lesser distance than that observed in a related doubly pyrazolate-bridged system described by Navarro et al [14] [3.924(3) Å] but by a greater distance than that observed for the doubly pyridazine-bridged system [3.760(2) Å] reported by Bremard et al [4]. The copper–copper separations observed in symmetric Schiff base macrocycles containing double phenolate (e.g. L2) rather than double pyridazine bridges are significantly shorter (typically 3.09–3.15 Å), due largely to the single atom nature of the phenolate bridge in comparison to the two atom bridge provided by pyridazine [11–13].

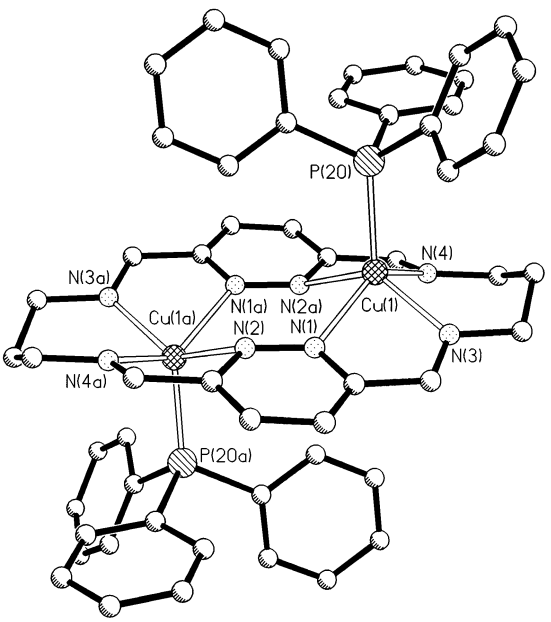

Fig. 6. Perspective view of the cation of **12**, $[Cu^{I}_{2}(L1)(PPh_3)_2]^{2+}$. Selected interatomic distances (Å) and angles (°): Cu(1)–N(3) 2.079(2), Cu(1)–N(4) 2.108(2), Cu(1)–N(1) 2.196(2), Cu(1)–P(20) 2.2239(8), Cu(1)–N(2a) 2.365(2), Cu(1)…Cu(1a) 4.4316(12), N(3)–Cu(1)–N(4) 89.52(8), N(3)–Cu(1)–N(1) 76.16(8), N(4)–Cu(1)–N(1) 136.15(7), N(3)–Cu(1)–P(20) 120.45(7), N(4)–Cu(1)–P(20) 103.50(6), N(1)–Cu(1)–P(20) 119.60(6), N(3)–Cu(1)–N(2a) 135.12(8), N(4)–Cu(1)–N(2a) 72.93(8), N(1)–Cu(1)–N(2a) 88.41(7), P(20)–Cu(1)–N(2a) 103.91(5).

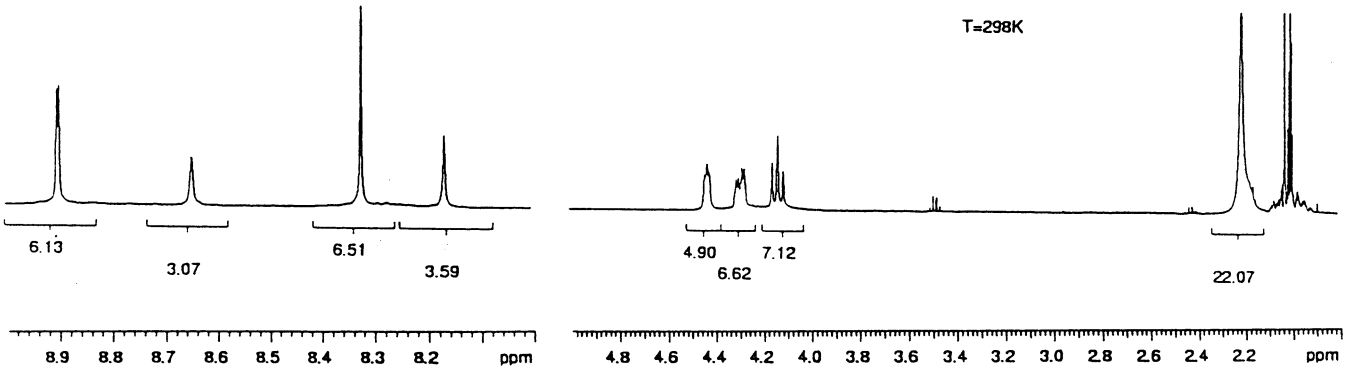

Fig. 7. ^{1}H-NMR of $[Cu^I_4(L1)_2]^{4+}$ (**10**) in CD_3CN at 298 K. Numbers underneath the signals indicate the relative signal integrations.

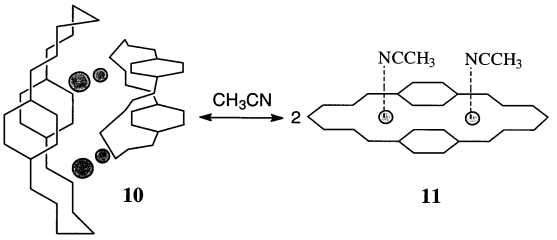

Fig. 8. Equilibrium between $[Cu^{I}_{4}(L1)_2]^{4+}$ (**10**) and $[Cu^{I}_{2}(L1)(MeCN)_2]^{2+}$ (**11**) in MeCN solution.

2.3. NMR spectroscopy

Simple ^{1}H-NMR spectra are obtained for the highly symmetrical tetracopper(I) grid complex $[Cu^{I}_{4}(L1)_2](PF_6)_4$ (**10**) in the non-coordinating solvents nitromethane and acetone [5]. However, in acetonitrile two sets of signals are obtained (Fig. 7), with the relative proportions of the two species varying with temperature. This indicates that there is an equilibrium between the tetracopper(I) grid complex and another species. The second species is believed to be the dicopper(I) complex $[Cu^{I}_{2}(L1)(MeCN)_2]^{2+}$ (**11**), with a structure similar to that of both $[Cu^{II}_{2}(L1)(MeCN)_2]^{4+}$ (**1**) and $[Cu^{II}Cu^{I}(L1)(MeCN)_2]^{3+}$ (**8**) (Fig. 8, Scheme 1) [5,8]. Consistent with this, over time the NMR signals become more complex and broaden out, presumably due to air oxidation of the dicopper(I) complex **11** which is expected to be more air sensitive than the parent grid complex **10**. Further support for the assignment of the second species as **11** comes from the NMR spectra of the dicopper(I) complex $[Cu^{I}_{2}(L1)(PPh_3)_2](PF_6)_2$ (**12**).

2.4. Magnetochemistry

Variable temperature magnetic susceptibility measurements were made on powdered samples of compounds **1**–**6** in the range 320 to 4.2 K (Table 1). The magnetic susceptibilities were observed to decrease to a minimum before rising sharply at low temperatures on account of a small concentration of monomer impurity. The corresponding values of magnetic moment decreased with decreasing temperature from ca. 1.2 μ_B per Cu at 320 to ca. 0.4 μ_B at 100 K below which they remained approximately constant. This behaviour is typical of strongly antiferromagnetically coupled systems. Fig. 9 shows a typical example, complex **3**.

The magnetic susceptibilities were fitted to the modified Bleaney Bowers equation (Eq. (1)) [15,16] where ρ is the fraction of monomeric impurity and $N\alpha$ is the temperature independent paramagnetism term.

$$x_A = \frac{N\beta^2 g^2}{3k(T-\Theta)}[1+\frac{1}{3}\exp(-2J/kT)]^{-1}(1-p)+\frac{[N\beta^2 g^2]p}{4kT}+N\alpha \quad (1)$$

An excellent fit was obtained in all cases and the best-fit paramater values are given in Table 1.

All complexes show strong antiferromagnetic coupling with rather similar J values. The pathway for this exchange is clearly the double pyridazine bridge and the important factor affecting the size of the exchange integral is the overlap of the copper d_{x2-y2} magnetic orbitals with the pyridazine N-donor p orbitals. The bonding geometries in **1** and **2** are similar (Cu–N–N = 127.3–129.2°) and thus the J values would be expected to be similar. Determining the effects on J of non-planarity or out-of-plane effects would require molecular orbital calculations of the type recently made by Thompson et al [16].

Comparison to detailed studies on acyclic μ-pyridazine bridged compounds by Thompson et al. [2,3] which also contain an exogenous bridging group, typically

Table 1
Results of fitting variable temperature data to the modified Bleaney Bowers equation (Eq. (1))

Sample	$-2J$ [a]/cm^{-1}	10^6Nα/cm^{-3}mol^{-1}	ρ [b]	g [c]	10^2R [d]
$[Cu_2(L1)](ClO_4)_4$ (**1**)	482	108 [e]	0.01	2.02	1.0
$[Cu_2(L1)Cl_2](ClO_4)_2$ (**2**)	464	60	0.06	2.00	2.1
$[Cu_2(L1)Br_2](ClO_4)_2$ (**3**)	492	60	0.02	2.15	1.3
$[Cu_2(L1)I_2](ClO_4)_2$ (**4**)	496	60	0.06	2.12	2.3
$[Cu_2(L1)(NCS)_2](ClO_4)_2$ (**5**)	532	60	0.02	2.02	1.1
$[Cu_2(L1)](NO_3)_2(H_2O)_2(ClO_4)_2$ (**6**)	412 [f]	60	0.02	2.10	2.0

[a] $+/-5$ cm^{-1}.
[b] $+/-0.002$.
[c] $+/-0.005$.
[d] $R = [\Sigma\,(/\chi_{obs}/-/\chi_{calc}/)T/\Sigma\,\chi_{obs}T]$ where T = temperature.
[e] Use of $N\alpha = 60 \times 10^{-6}$ cm^3 mol^{-1} gives a higher R value (5.9) and an unreasonably low g (1.86) with $-2J = 416$ cm^{-1}.
[f] Fitted in the range 100–300 K only.

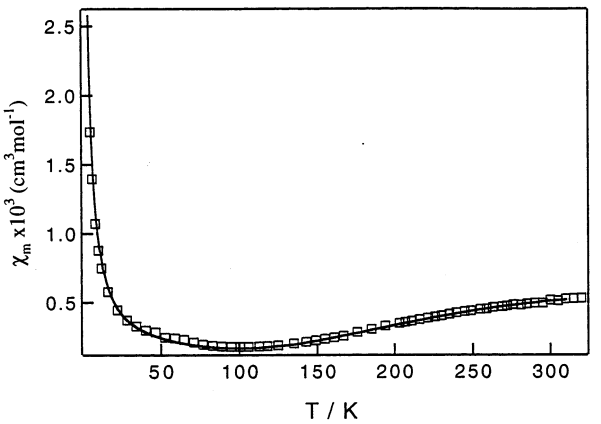

Fig. 9. Plot of magnetic susceptibility versus temperature for $[Cu_2(L1)Br_2](ClO_4)_2$ (**3**). The solid line is calculated using the best-fit parameters given in Table 1.

Table 2
Summary of electrode potentials versus SCE and K_c values

		$2Cu^{II} \rightarrow Cu^{II}Cu^{I}$		$Cu^{II}Cu^{I} \rightarrow 2Cu^{I}$		
Sample	Solvent	$E_{1/2}$/V	Reversible	$E_{1/2}$/V	Reversible	K_c
$[Cu_2(L1)](ClO_4)_4$ (**1**)	MeCN	+0.43	Yes	+0.10	Yes	$3.8x10^5$
$[Cu_2(L1)Br_2](ClO_4)_2$ (**3**)	MeCN	+0.39	Yes	+0.01	No	$2.7x10^6$
$[Cu_2(L1)I_2](ClO_4)_2$ (**4**)	MeCN	+0.45	No	+0.04	Yes	$8.6x10^6$
$[Cu_2(L1)(NCS)_2](ClO_4)_2$ (**5**)	MeCN	+0.44	Yes	+0.04	Yes	$5.8x10^6$
$[Cu_2(L1)(H_2O)_2](ClO_4)_4$ (**7**)	MeCN	+0.41	Yes	+0.08	Yes	$3.8x10^5$
$[Cu_2(L1)Cl_2](ClO_4)_2$ (**2**)	H_2O	+0.07	No	−0.14	No	$3.6x10^3$
$[Cu_2(L1)(H_2O)_2](ClO_4)_4$ (**7**)	H_2O	+0.08	No	−0.14	No	$5.2x10^3$

hydroxide, confirm the present values of the exchange integral in relation to the bridging geometry and copper–copper separation. Thus, examples of μ-pyridazine ligands which generate five-membered chelate rings on coordination, similar to the series of complexes currently under discussion, yield μ-hydroxo complexes with copper–copper distances of ca. 3.42 Å and $-2J$ values of 760 to 790 cm^{-1}, the μ-(OH) bridge having a significant influence on the bridge geometry and on the exchange integral. The complex most closely related to our series of doubly pyridazine bridged complexes is a planar acyclic oxime complex which also contains two pyridazine bridges [4]. The copper–copper separation of 3.760(2) Å and the Cu–N–N(pyridazine) angle of 126.8(7)° are similar to that of $[Cu_2(L1)(MeCN)_2](ClO_4)_4$ [3.805(3) Å and 128.4(2)°], as is the $-2J$ value, 536 cm^{-1}.

2.5. Electrochemistry and spectroelectrochemistry

2.5.1. Electrochemistry of dicopper(II) complexes 1–7

The dicopper(II) compounds, **1**–**7**, were investigated by cyclic voltammetry (Table 2). The studies on the complexes **1**, **3**, **4** and **7** were carried out in both acetonitrile and aqueous solution. Complexes **2** and **6** were studied only in aqueous solution due to a lack of solubility in acetonitrile, and complex **5** was studied only in acetonitrile. The limited solubility of complex **3** in acetonitrile and of complex **1** in water meant that saturated solutions, of concentration less than 1×10^{-3} mol l^{-1}, had to be used in these cases. All potentials quoted in this section are versus SCE unless otherwise stated. The reversibility of the redox couples was judged against the usual criteria [17].

The cyclic voltammograms obtained in acetonitrile showed the same general pattern of two separate one electron redox couples associated with the $Cu_2^{II}(L1)$ to $Cu^{I}Cu^{II}(L1)$ and $Cu^{I}Cu^{II}(L1)$ to $Cu_2^{I}(L1)$ redox processes [e.g. Fig. 10(a), Table 2]. Specifically, the voltammograms of **1** and **5** showed two fully reversible redox couples at positive electrode potentials. For the thiocyanate complex **5** an additional large broad peak at +0.70 V was observed which was, after comparison with the electrochemistry of a sodium thiocyanate solution, assigned to the redox

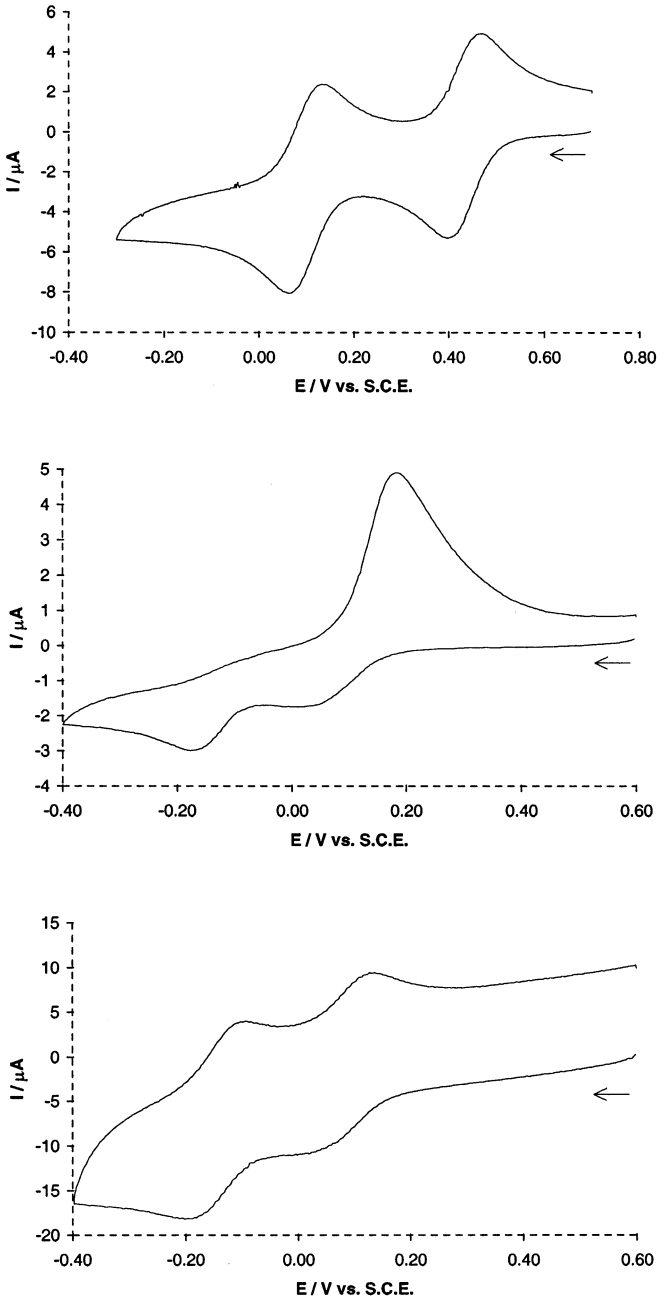

Fig. 10. Cyclic voltammograms, versus SCE, of $[Cu_2^{II}(L1)](ClO_4)_4$ (**1**) (a) in acetonitrile, scan rate 0.1 V s^{-1} (b) in water, scan rate 0.025 V s^{-1} (c) in water, scan rate 1 V s^{-1}.

activity of NCS^-. The two redox couples observed for the bromide complex **3** occurred at slightly lower potentials than those observed for **1**, and whilst the couple with $E_{1/2} = 0.39$ V is fully reversible, the couple with $E_{1/2} = 0.01$ V is only quasi-reversible. The converse is true for the iodide complex **4**, in which a fully reversible redox couple occurred at $E_{1/2} = 0.04$ V and a quasi-reversible couple at $E_{1/2} = 0.45$ V. The presence of I^- in **4** leads to two other redox processes occurring in the range -0.40 to $+0.80$ V. These redox couples, with $E_{1/2} = 0.27$ and $E_{1/2} = 0.64$ V, were assigned to the redox activity of the anion (comparison with a voltammogram of an acetonitrile solution of tetraethylammonium iodide showed peaks in very similar positions) [3].

Whilst there were many similarities between the cyclic voltammograms obtained in acetonitrile and those obtained in water at high scan speeds, in water at lower scan speeds significant surface activity was generally observed, as might be expected. This point is nicely illustrated by the behaviour of complex **1** in water (10b,c). At 25–100 mV s^{-1} a stripping wave is observed at $+0.18$ V, whereas at 200–1000 mV s^{-1} a cyclic voltammogram similar to that obtained in acetonitrile is observed, although the processes are now only quasi-reversible ($+0.07$ and -0.15 V). An aqueous solution of **2** gave a voltammogram with two broad redox couples, one at positive ($+0.07$ V) and one at negative (-0.14 V) potentials. Whilst the peak separation was constant, the relative peak heights and their variation with respect to scan rate indicated that neither of the processes are fully reversible. No stripping waves were observed at any of the scan speeds investigated, 25–1000 mV s^{-1}, in this case or in the case of complex **7** ($+0.08$ and -0.14 V). The bromide complex **3** and the nitrate complex **6**, in water, gave very similar voltammograms to those of **1**, whilst the iodide complex **4** yielded complicated cyclic voltammograms (due in part to the presence of I^- redox processes) with surface activity observed at all accessible scan rates (up to 1 V s^{-1}).

In related pyridazine or phthalazine bridged dicopper(II) complexes additional halide, hydroxy or azide bridges are often present [2,3]. They typically undergo a single two electron redox process at positive potentials, ca. $+0.2$ to $+0.8$ V versus SCE [3], which is similar to the potential of the first redox process for each of our doubly bridged pyridazine complexes. However, with our macrocyclic ligand two one electron processes are observed and as a result the mixed valence $Cu^{II}Cu^{I}$ species is accessible. Two such examples, the mixed valent complexes **8** and **9**, have been isolated and structurally characterised (vide infra) [5]. This has not been observed before in pyridazine bridged systems but is well established in the related phenolate bridged dicopper(II) complexes of macrocycles like L2 which typically undergo two one electron reductions at lower potentials [12,13]. The softer nitrogen donors provided by the pyridazine bridges clearly provide more favourable donors for Cu^{I} [3] and therefore the reductions occur at more positive potentials, however, in common with the phenolate-bridged analogues, the two processes are well separated. An indication of the stability of a mixed valence state is given by the comproportionation constant K_c. The K_c values for these and related complexes are listed in Table 2. Complexes **1**, **3**, **4**, and **5** all have K_c values similar to each other and to the value reported for the macrocyclic phenolate complex $[Cu_2(L2–2H)]^{2+}$

[13]. As expected, destabilisation of the mixed valence species is observed in aqueous solution.

*2.5.2. Spectroelectrochemistry of **1***

In order to count the electrons transferred and to access the mixed valent oxidation state, spectroelectrochemical experiments were undertaken on acetonitrile solutions of $[Cu^{II}_2(L1)](ClO_4)_4$ (**1**). The results of the controlled potential electrolyses are detailed in Fig. 11. Bulk electrolysis of a green solution of $[Cu^{II}_2(L1)](ClO_4)_4$ at a potential of 0.00 V versus 0.01 mol l^{-1} $AgNO_3$/Ag resulted in the transfer of 0.97 electron equivalents and the formation of the mixed valence, formally copper(I)/copper(II), species. In addition, the solution became yellow–brown coloured, with a new band centred at 450 nm, along with a band of increased absorbance at 380 nm. No clearly assignable intervalence charge transfer band was observed. This UV–vis spectrum is identical to that of the subsequently isolated mixed valent complex **8**.

On decreasing the potential further, to -0.30 V versus 0.01 mol l^{-1} $AgNO_3$/Ag, the solution remains yellow–brown, a second electron is added (0.93 electron equivalents) and a single intense absorbance in the visible, centred on 410 nm, results. As the species present is now a dicopper(I) complex this band is presumably due to a charge transfer transition. A similar UV–vis spectrum is obtained for the triphenylphosphine derivative, **12**, of this dicopper(I) complex.

The clean isobestic points indicate that both the mixed valent complex and the dicopper(I) complex are reasonably stable under an argon atmosphere at room temperature (r.t.), the experimental conditions employed in this study. Subsequently both mixed valent, **8** and **9**, and dicopper(I), **12**, complexes have been isolated and structurally characterised (vide infra).

As noted above, the successful generation of the mixed valent copper(II)/copper(I) state is unprecedented in the chemistry of pyridazine bridged complexes. All previous examples of pyridazine bridged dicopper(II) complexes undergo one two-electron reduction, however, the dicopper(II) complex of macrocycles such as L2 undergo two successive redox processes. Gagné and co-workers were able to isolate and crystallise the mixed valent complex of L2, and the X-ray structure determination revealed that one of the copper centres, probably the copper(II) ion, was square planar whilst the other centre, probably the copper(I) ion, was square pyramidal [13]. The fact that the two copper sites are inequivalent indicates that the electron is localised on one of the two copper ions in the solid state, however, EPR studies have revealed that in solution at r.t. the electron is delocalised over both sites whereas at low temperatures it is localised on one site (Class II) [13]. Our mixed valent complex, **8**, also has two different copper sites corresponding to localised valences so at low temperature in the solid state it is a Class I complex [5].

To probe the nature of the mixed valent complex further, a variable temperature EPR study was undertaken of the electrochemically generated complex (in MeCN). This revealed that at low temperatures (80 K) the unpaired electron was localised on one of the two copper ions, as a four line rhombic spectrum typical of a distorted square pyramidal copper(II) ion ($I = 3/2$) was obtained [Fig. 12(a),

$g_z = 2.22$; g_y, $g_x = 2.06$, 2.00]. Therefore it is a Class I mixed valence complex at low temperatures. The temperature was then increased to close to, and above, the melting point of the sample. Coalescence of the frozen-solution pattern occurred as expected, but it remained incomplete and the anisotropic splittings of the g values and hyperfine lines did not collapse entirely. In the given solvent, the spin system apparently did not reach the regime of fast molecular tumbling with respect to the

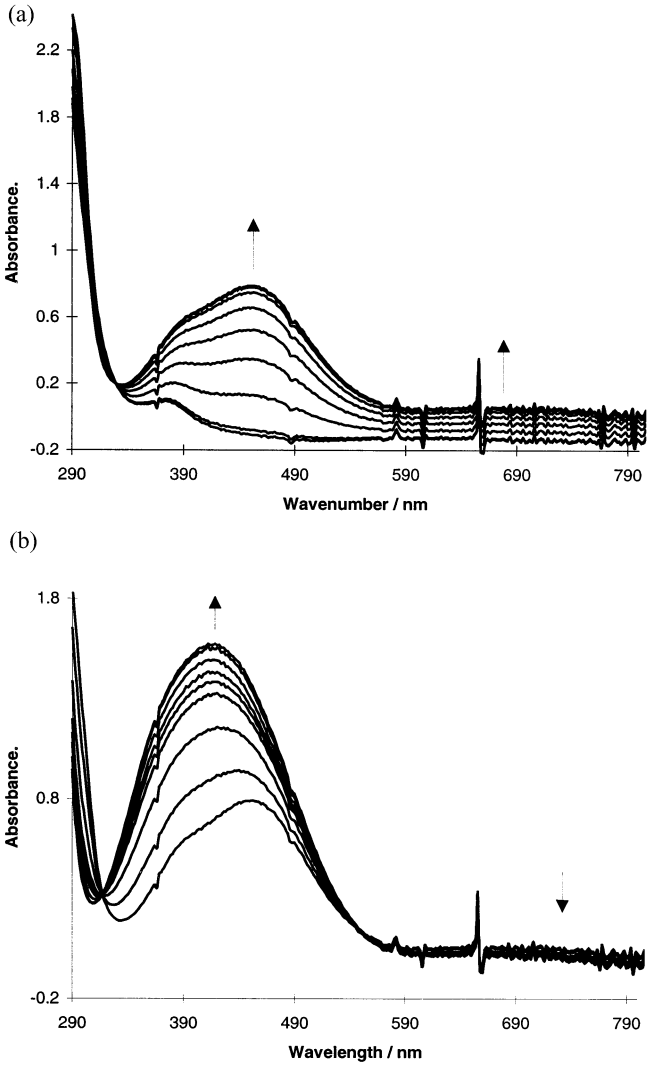

Fig. 11. UV–vis spectra recorded at r.t. for a 0.4 mmol l^{-1} $[Cu_2^{II}(L1)](ClO_4)_4$ (**1**), 1 mol l^{-1} tetrabutylammonium perchlorate, acetonitrile solution during bulk electrolyses versus 0.01 mol l^{-1} $AgNO_3$/Ag (a) at a potential of 0.0 V, $Cu(II)_2 \rightarrow Cu(II)Cu(I)$ (b) at a potential of -0.3 V, $Cu(II)Cu(I) \rightarrow Cu(I)_2$. The Fc/Fc^+ couple occurred at $+0.084$ V in this system.

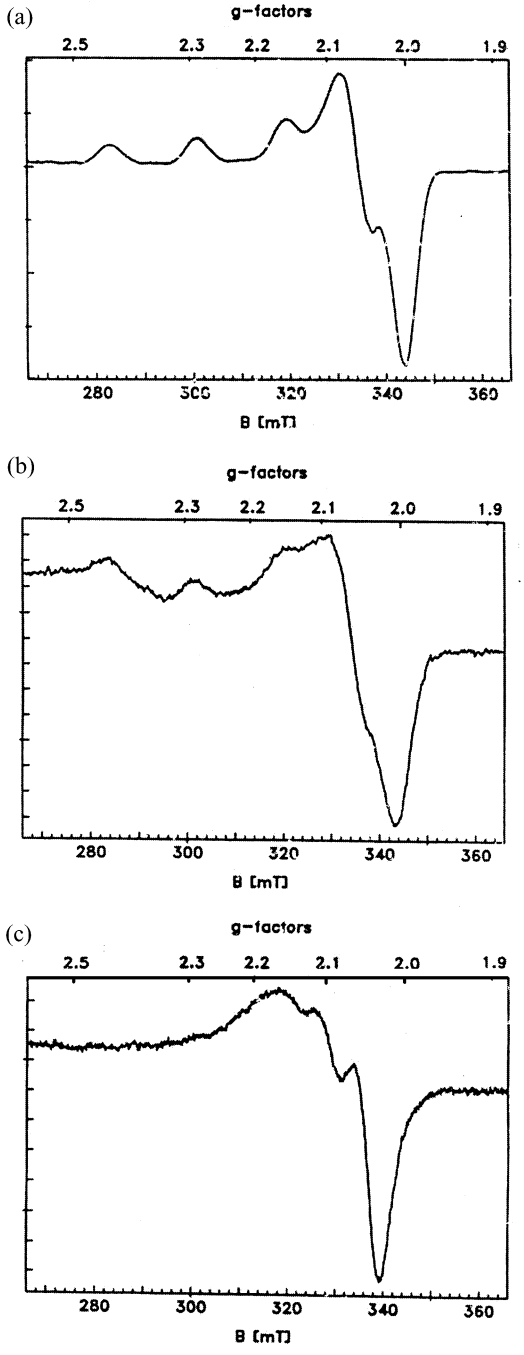

Fig. 12. EPR spectra of electrochemically generated $Cu_2(L1)^{3+}$ in an acetonitrile electrolyte solution at (a) 80K (b) at 220K (c) at 240K.

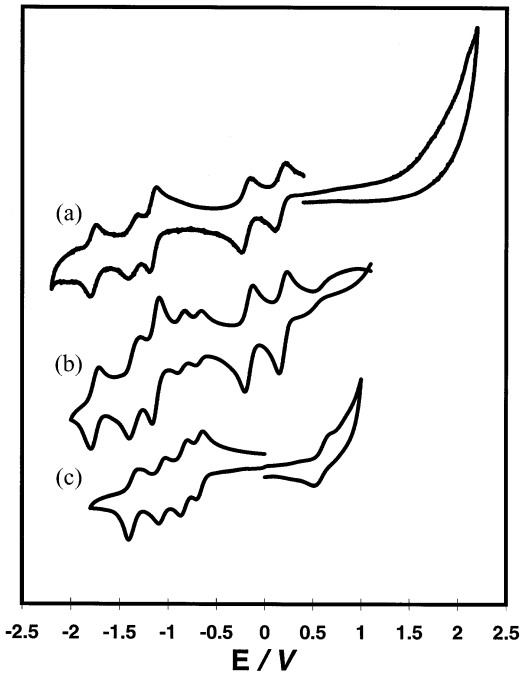

Fig. 13. Cylic voltammograms, versus 0.01 M $AgNO_3$/Ag, of (a) $[Cu^{II}_2(L1)(MeCN)_2](ClO_4)_4$ (**1**)•2MeCN in acetonitrile, scan rate 100 mV s^{-1} (b) $[Cu^{I}_4(L1)_2](PF_6)_4$ (**10**) in acetonitrile, scan rate 200 mV s^{-1} (c) $[Cu^{I}_4(L1)_2](PF_6)_4$ **10** in acetone, scan rate 200 mV s^{-1}.

high frequencies corresponding to these intrinisic splittings. Due to this signal coalescence it was not possible to observe isotropic hyperfine splitting in order to determine whether the electron remains localised on one copper centre or becomes delocalised across both copper centres at temperatures above the melting point of the acetonitrile solution. However, the electronic spectrum indicates that the mixed valence species is Class I at r.t.

*2.5.3. Electrochemistry of mixed valent complex **8** and copper(I) complexes **10** and **11***

In this section all potentials are quoted versus 0.01 M $AgNO_3$/Ag. The mixed valent complex $[Cu^{II}Cu^{I}(L1)(MeCN)_2](ClO_4)_2(PF_6)$ (**8**) has a very similar cyclic voltammogram in acetonitrile to that observed for $[Cu^{II}_2(L1)(MeCN)_2](ClO_4)_4$ (**1**)•2MeCN. Controlled potential coulometry confirmed that complex **8** is indeed mixed valent [at $+0.75$ V, 0.82 electron equivalents were transferred ($I_f = 1\%\ I_i$)]. A full scan range cyclic voltammogram of **1** in acetonitrile is shown in Fig. 13: in addition to the two metal centred processes described in the previous section, $Cu^{II}_2(L1)$ to $Cu^{I}Cu^{II}(L1)$ ($+0.20$ V) and $Cu^{I}Cu^{II}(L1)$ to $Cu^{I}_2(L1)$ (-0.15 V), it should be noted that there are three further waves at more negative potentials which are believed to correspond to ligand reductions [6].

The tetracopper(I) complex **10** was investigated in both acetonitrile and acetone, due to the differing NMR spectra obtained in these two solvents (Figs. 7 and 8, vide infra). In acetonitrile, eight processes are observed: the five waves seen before for **1**•2MeCN plus three new waves (Fig. 13). These are believed to be due to the presence of an equilibrium mixture of the tetracopper(I) grid complex $[Cu^{I}_{4}(L1)_2]^{4+}$ (**10**) and the dicopper(I) complex $[Cu^{I}_{2}(L1)(MeCN)_2]^{2+}$ (**11**). Complex **11** is expected to have the same cyclic voltammogram as **1**•2MeCN, and this is observed. Superimposed on this are an extra pair of clearly discernable processes at -0.69 and -0.87 V, and an irreversible oxidation process at $+0.77$ V, which are due to the presence of intact complex **10**.

In acetone only five waves are observed within the accessible solvent window (Fig. 13). The pair of metal centred processes, at $+0.20$ and -0.15 V, assigned to the presence of equilibrium amounts of **11**, are absent, which is consistent with the expected presence of only the tetracopper(I) grid complex **10** in acetone (vide infra). As in acetonitrile, the presence of **10** leads to observation of an oxidation process, at $+0.60$ V (now quasi-reversible), along with waves at -0.67 V (controlled potential electrolysis at -0.756 V resulted in the transfer of 0.82 electron equivalents) and -0.84 V, and further reduction waves at more negative potentials.

3. Conclusion

Transmetallation of a pyridazine-containing L1′ Schiff-base macrocycle with copper(II) has led to the formation of $[Cu_2(L1)](ClO_4)_4$ (**1**). Use of **1** in anion replacement reactions has allowed the isolation of a series of dicopper(II) complexes of the corresponding L1 macrocycle. X-ray structure determinations of three representative complexes and mass spectrometry results confirm that ring contraction from L1′ to L1 has occurred in all cases. In each case the copper(II) ions are doubly bridged by pyridazine and exhibit strong antiferromagnetic coupling ($-2J$ 412 cm^{-1} to 532 cm^{-1}). In addition, two one-electron reductions at positive potentials (versus SCE) are exhibited by all of the compounds, in contrast to all previously studied pyridazine bridged copper complexes. The mixed valent copper(II)copper(I) species are stable as evidenced by (a) the K_c values obtained in acetonitrile (3.8×10^5 to 8.6×10^6), (b) the successful electrochemical generation of this state in the case of complex **1** and (c) the subsequent synthesis and isolation of it as an air stable solid, **8**. The observation, by NMR spectroscopy, of an equilibrium between the fully characterised tetracopper(I) grid complex **10** and the proposed dicopper(I) complex **11** led to the fully reduced dicopper(I) complex $[Cu^{I}_{2}(L1)(PPh_3)_2](PF_6)_2$ (**12**) being fully characterised. Studies of the coordination chemistry of L1, and related ligands, with other transition metal ions are well underway [9].

4. Experimental

4.1. Measurements

As reported previously [7] except for the following. FAB Mass spectra were recorded at the University of Canterbury using a Kratos MS80 RFA mass spectrometer. Electrochemistry and spectroelectrochemistry was carried out, with 1 mmol l^{-1} solutions and 0.1 mol l^{-1} tetraethylammonium perchlorate supporting electrolyte, on an EG&G Princeton Applied Research 273A potentiostat, using either a saturated calomel electrode (SCE, Section 2.5.1) or a 0.01 mol l^{-1} $AgNO_3$/Ag reference electrode (Section 2.5.3). Spectroelectrochemical and EPR measurements on **1** (Section 2.5.2) were made at the MPI for Strahlenchemie. The same conditions as above were used for these studies except that tetrabutylammonium hexafluorophosphate supporting electrolyte and 0.01 mol l^{-1} $AgNO_3$/Ag reference electrode were used. The electrochemically produced mixed valent species (controlled potential coulometry) was examined using a Bruker ESP300 continuous wave X-band EPR spectrometer equipped with an Oxford Instruments ESR900 helium flow cryostat. Magnetic susceptibility studies were carried out at Monash University using a Quantum Design MPMS SQUID magnetometer with an applied field of 1 T. The powdered sample was contained in a calibrated gelatine capsule which was held in the centre of a soda straw fixed to the end of the sample rod. The magnetization values of the instrument were calibrated against a standard palladium sample, supplied by Quantum Design, and also against chemical calibrants such as $CuSO_4.5H_2O$ and $[Ni(en)_3](S_2O_3)$.

4.2. Materials

Acetonitrile (HPLC grade) was dried before use (CaH_2). Acetone (HPLC grade) was used without further purification. Sodium thiocyanate and tetraethylammonium perchlorate were recrystallised from water. 1,3-Diaminopropane was distilled from NaOH. $Pb_2(L1')(ClO_4)_4$, $[Cu^{II}Cu^{I}(L1)(MeCN)_2](ClO_4)_2(PF_6)$ (**8**) and $[Cu^{I}_4(L1)_2](PF_6)_4$ (**10**) were prepared as reported previously [5,7].

Caution: Whilst no problems were encountered in the course of this work perchlorate mixtures are potentially explosive and should therefore be handled with appropriate care.

4.3. Synthesis

4.3.1. *$[Cu_2(L1)](ClO_4)_4$ (1)*

$[Pb_2(L1')](ClO_4)_4$ (0.873 g, 0.58 mmol) was suspended in acetonitrile (250 ml) and heated until the solid dissolved. To this stirred solution a solution of $Cu(ClO_4)_2.6H_2O$ (0.9 g, 2.43 mmol) in acetonitrile (20 ml) was added dropwise. The clear yellow solution initially turned dark brown, transforming to a deep emerald green approximately half way through the addition. The solution was then left to stir for 15 min. at r.t. before being reduced in volume to ca. 50 ml in vacuo. The

green single crystals of $[Cu_2(L1)(MeCN)_2](ClO_4)_4$ suitable for X-ray analysis, obtained by vapour diffusion of diethyl ether into the resulting acetonitrile solution, were filtered off and dried in vacuo to yield $[Cu_2(L1)](ClO_4)_4$ (0.794 g, 76%) as a green powder. Found: C, 24.7; H, 2.4; N, 12.7. $[Cu_2(L1)](ClO_4)_4$ requires C, 24.8; H, 2.3; N, 12.8%.IR (KBr disk, inter alia) 3465 (m), 3066 (m), 2971 (m), 2943 (m), 1649 (m), 1590 (m), 1556 (m), 1093 (s), 630 (s) cm^{-1}. Mass spectrum m/z 674 $[Cu_2(L1)(ClO_4)_2]^+$, 573 $[Cu_2(L1)ClO_4]^+$, 474 $[Cu_2(L1)]^+$, 411 $[Cu(L1)]^+$. UV–vis: in acetonitrile $\lambda = 600$ nm ($\varepsilon = 80$ mol l^{-1} cm^{-1}), $\lambda = 375$ ($\varepsilon = 680$ mol l^{-1} cm^{-1}); in water $\lambda = 600$ nm ($\varepsilon = 70$ mol $l^{-1}cm^{-1}$). Conductivity: in acetonitrile $\Lambda = 375$ mol^{-1} cm^2 Ω^{-1} (3:1 340–420); in water $\Lambda = 447$ mol^{-1} cm^2 Ω^{-1} (4:1 = 450–510) [18].

4.3.2. *$[Cu_2(L1)Cl_2](ClO_4)_2$* (**2**)

$[Cu_2(L1)](ClO_4)_4$ (0.524 g, 0.6 mmol) was dissolved in acetonitrile (100 ml) and to this stirred solution a solution of tetraethylammonium chloride (0.220 g, 1.2 mmol) in ca. 10 ml acetonitrile was added dropwise. The green solution lightened in colour and an olive precipitate formed. The suspension was stirred for a further 90 min. before being filtered and dried in vacuo. Recrystallisation by vapour diffusion of diethyl ether into a dimethylformamide solution yielded dark brown crystals of $[Cu_2(L1)Cl_2(H_2O)](ClO_4)_2$ suitable for X-ray analysis (0.390 g, 87%). Found: C, 29.0; H, 2.7; N, 15.0. $[Cu_2(L1)Cl_2](ClO_4)_2$ requires C, 29.1; H, 2.8; N, 15.1%. IR (KBr disk, inter alia) 3052 (m), 2947 (m), 2853 (m), 1652 (m), 1613 (m), 1588 (m), 1558 (m), 1120 (s), 1078 (s), 625 (s) cm^{-1}. Mass spectrum m/z 675 $\{[Cu_2(L1)](ClO_4)_2\}^+$, 610 $\{[Cu_2(L1)Cl]ClO_4\}^+$, 573 $\{[Cu_2(L1)]ClO_4\}^+$, 511 $\{[Cu(L1)]ClO_4\}^+$, 474 $[Cu_2(L1)]^+$, 411 $[Cu(L1)]^+$. UV–vis: in water $\lambda = 475$ nm ($\varepsilon = 600$ mol l^{-1} cm^{-1}).

4.3.3. *$[Cu_2(L1)Br_2](ClO_4)_2$* (**3**)

$[Cu_2(L1)](ClO_4)_4$ (0.022 g, 0.025 mmol) was dissolved in acetonitrile (25 ml) and to this stirred green solution a solution of tetraethylammonium bromide (0.011 g, 0.05 mmol) in ca. 10 ml acetonitrile was added dropwise. The resulting solution immediately lightened to an olive green colour. The solution was stirred for a further 12 h, after which time a small amount of light green precipitate had formed. Due to difficulties encountered in filtering this fine precipitate the suspension was centrifuged and the clear olive supernatant liquid decanted off. This solution was then reduced in volume in vacuo to ca. 5 ml, at which time a red precipitate formed. The precipitate was filtered, washed with acetonitrile and diethyl ether and dried in vacuo (0.011 g, 53%). Found: C, 25.8; H, 2.6; N, 13.3. $[Cu_2(L1)Br_2](ClO_4)_2$ requires C, 25.9; H, 2.4; N, 13.4%. IR (KBr disk, inter alia) 3043 (m), 2961 (m), 1644 (m), 1614 (m), 1588 (m), 1554 (m), 1124 (s), 1071 (s), 622 (s) cm^{-1}. Mass spectrum m/z 654 $[Cu_2(L1)Br_2ClO_4]^+$, 573 $[Cu_2(L1)ClO_4]^+$, 555 $[Cu_2(L1)Br]^+$, 510 $[Cu_2(L1)]^+$, 474 $[Cu_2(L1)]^+$, 411 $[Cu(L1)]^+$. UV–vis: in water $\lambda = 460$ nm ($\varepsilon = 225$ mol l^{-1} cm^{-1}), $\lambda = 350$ nm ($\varepsilon = 855$ mol l^{-1} cm^{-1}). Conductivity: in water $\Lambda = 284$ mol^{-1} cm^2 Ω^{-1} (2:1 210-250, 3:1 340–380) [18].

*4.3.4. $[Cu_2(L1)I_2](ClO_4)_4$ (**4**)*

$[Cu_2(L1)](ClO_4)_4$ (0.022 g, 0.025 mmol) was dissolved in acetonitrile (25 ml) and to this stirred green solution a solution of tetraethylammonium iodide (0.013 g, 0.05 mmol) in ca. 10 ml acetonitrile was added dropwise. The solution immediately turned a deep brown colour and was allowed to stir for 5 h. The volume of the solution was then reduced in vacuo to ca. 10 ml and crystals were obtained by vapour diffusion of diethyl ether into this solution over two days. The small dark brown crystalline blocks, which were not suitable for X-ray analysis, were filtered and dried in vacuo (0.012 g, 52%). Found: C, 23.5; H, 2.2; N, 12.1. $[Cu_2(L1)I_2](ClO_4)_2$ requires C, 23.4; H, 2.2; N, 12.1%. IR (KBr disk, inter alia) 3056 (m), 2988 (m), 2938 (m), 2841 (m), 1640 (m), 1589 (m), 1556 (m), 1092 (s), 624 (s) cm^{-1}. Mass spectrum m/z 700 $[Cu_2(L1)ICl O_4]^+$, 601 $[Cu_2(L1)I]^+$, 573 $[Cu_2(L1)ClO_4]^+$, 511 $[Cu_2(L1)]^+$, 474 $[Cu_2(L1)]^+$, 411 $[Cu(L1)]^+$. UV–vis: in acetonitrile $\lambda = 680$ nm ($\varepsilon = 405$ mol l^{-1} cm^{-1}). Conductivity: in acetonitrile $\Lambda = 347$ mol^{-1} cm^2 Ω^{-1} (3:1 340–420) [18].

*4.3.5. $[Cu_2(L1)(NCS)_2](ClO_4)_2$ (**5**)*

$[Cu_2(L1)](ClO_4)_4$ (0.131 g, 0.15 mmol) was dissolved in acetonitrile (25 ml) and to this stirred green solution a solution of sodium thiocyanate (0.024 g, 0.3 mmol) in ca. 10 ml acetonitrile was added dropwise. A mustard precipitate immediately formed. The suspension was stirred for a further 30 min. and the solid was then filtered, washed with acetonitrile and dried in vacuo (0.085 g, 75%). Found: C, 30.5; H, 2.4; N, 18.0; S, 9.0. $[Cu_2(L1)(NCS)_2](ClO_4)_2$ requires C, 30.4; H, 2.5; N, 17.7; S, 8.1%. IR (KBr disk, inter alia) 3039 (m), 2996 (m), 2949 (m), 2921 (m), 2851 (m), 2068 (s), 2047 (s), 1640 (m), 1587 (m), 1552 (m), 1191 (s), 1090 (s), 637 (m), 625 (s) cm^{-1}. Mass spectrum m/z 631 $[Cu_2(L1)NCSClO_4]^+$, 573 $[Cu_2(L1)ClO_4]^+$, 532 $[Cu_2(L1)NCS]^+$, 474 $[Cu_2(L1)]^+$, 411 $[Cu(L1)]^+$.

*4.3.6. $[Cu_2(L1)](NO_3)_2(H_2O)_2(ClO_4)_2$ (**6**)*

A blue acetonitrile solution (10 ml) of $Cu(NO_3)_2.3H_2O$ (0.024 g, 0.1 mmol) was added dropwise to a stirred solution of $[Cu_2(L1)](ClO_4)_4$ (0.087 g, 0.1 mmol) in acetonitrile (25 ml). This green solution was left to slowly evaporate. After 2 weeks the resulting dark green crystals, too small for X-ray analysis, were filtered off and dried in vacuo (0.041 g, 49%). Found: C, 25.9; H, 2.7; N, 16.5. $[Cu_2(L1)](NO_3)_2(H_2O)_2(ClO_4)_2$ requires C, 25.9; H, 2.9; N, 16.8%. IR (KBr disk, inter alia) 3486 (s), 3062 (m), 3011 (m), 2965 (m), 1651 (m), 1590 (m), 1559 (m), 1385 (s), 1324 (s), 1082 (s), 628 (s) cm^{-1}. Mass spectrum m/z 674 $\{[Cu_2(L1)](ClO_4)_2\}^+$, 637 $[Cu_2(L1)NO_3ClO_4]^+$, 573 $[Cu_2(L1)ClO_4]^+$, 538 $[Cu_2(L1)NO_3]^+$, 489 $[Cu_2(L1)H_2O]^+$, 474 $[Cu_2(L1)]^+$. UV–vis: in water $\lambda = 600$ nm ($\varepsilon = 55$ mol l^{-1} cm^{-1}), $\lambda = 351$ nm ($\varepsilon = 530$ mol l^{-1} cm^{-1}). Conductivity: in water $\Lambda = 446$ mol^{-1} cm^2 Ω^{-1} (3:1 450–510) [18].

*4.3.7. $[Cu_2(L1)(H_2O)_2](ClO_4)_4$ (**7**)*

An acetonitrile solution (5 ml) of pyridazine (0.008 g, 0.1 mmol) in acetonitrile (5 ml) was added dropwise to a green solution of $[Cu_2(L1)](ClO_4)_4$ (0.087 g, 0.1 mmol)

in acetonitrile (25 ml). The solution was refluxed for 20 min. during which time it darkened significantly from emerald green to dark brown. After cooling to r.t. the solvent volume was reduced in vacuo to 15 ml and divided into two equal aliquots. $NaClO_4$ (ca. 0.5 g) was added to each aliquot and the brown solutions left to slowly to evaporate. The resulting brown single crystals were suitable for X-ray analysis. In order to carry out a full characterisation another sample was prepared in an identical fashion, only the brown crystals were filtered off, washed carefully with acetonitrile and dried in vacuo (0.038 g, 42%). Found: C, 23.9; H, 2.5; N, 12.0. $[Cu_2(L1)(H_2O)_2](ClO_4)_4$ requires C, 23.8; H, 2.7; N, 12.3%. IR (KBr disk, inter alia) 3433 (s), 3065 (m), 2937 (m), 1638 (m), 1591 (m), 1546 (m), 1087 (s), 622 (s) cm^{-1}. Mass spectrum m/z 674 $[Cu_2(L1)(ClO_4)_2]^+$, 613 $[Cu_2(L1)(H_2O)_2ClO_4]^+$, 573 $[Cu_2(L1)ClO_4]^+$, 489 $[Cu_2(L1)H_2O]^+$, 474 $[Cu_2(L1)]^+$.

*4.3.8. $[Cu^{II}Cu^{I}(L1)(NCS)_4Cu^{I}]MeCN$ (**9**)*

Method (a): Single crystals can be obtained from this synthesis. To a stirred solution of $Cu^{II}Cu^{I}(L1)(PF_6)(ClO_4)_2$ (0.119 g, 0.145 mmol) dissolved in acetonitrile (20 ml) was added, dropwise over 5 min., NaNCS (0.037 g, 0.459 mmol) in acetonitrile (7 ml). The solution was filtered and the filtrate left to stand in an open beaker. This afforded dark brown single crystals over a few days. These were filtered off and dried in vacuo (0.0189 g, 28%). Method (b): Stoichiometric synthesis. Solid $Cu(MeCN)_4PF_6$ (0.021 g, 0.056 mmol) was added to a 50 ml acetonitrile solution of $Cu^{II}Cu^{I}(L1)(PF_6)(ClO_4)_2.2MeCN$ (0.051 g, 0.056 mmol). To this stirred solution was added dropwise a 20 ml solution of NaSCN (0.018 g, 0.22 mmol). The mixture was stirred for 2 h, and on standing overnight the volume was reduced by slow evaporation to ca. 40 ml. The dark brown solid that formed was filtered off and dried in vacuo to yield **9** (0.027 g, 59%). Found C, 35.3; H, 2.8; N, 22.5. $C_{24}H_{23}N_{13}Cu_3S_4$ requires C, 35.5; H, 2.8; N, 22.4%. IR (KBr disk, inter alia) 3441 (m), 3048 (w), 2926 (m), 2839 (w), 2081(s), 1648 (m), 1568 (m), 1554 (w), 1316 (m) cm^{-1}. Mass spectrum m/z 711 $[Cu_3(L1)(NCS)_3]^+$, 590 $[Cu_2(L1)(NCS)_2]^+$, 532 $[Cu_2(L1)NCS]^+$.

*4.3.9. $[Cu^{I}_2(L1)(PPh_3)_2](PF_6)_2$ (**12**)*

Under a nitrogen atmosphere, solid 3,6-diformylpyridazine (0.070 g, 0.51 mmol) and $Cu(MeCN)_4PF_6$ (0.191 g, 0.51 mmol) were added to 30 ml of acetonitrile. A 20 ml acetonitrile solution of 1,3-diaminopropane (0.038 g, 0.51 mmol) was added dropwise to this light yellow mixture which immediately turned dark brown. This solution was stirred overnight, solid triphenylphosphine (0.132 g, 0.50 mmol) added, and the solution stirred for a further hour. The resulting solution was filtered, in air, and dark brown single crystals of **12** were obtained by vapour diffusion of diethyl ether into the acetonitrile filtrate (0.165 g, 51% yield). Found: C, 50.2; H, 3.8; N, 8.9. $C_{54}H_{50}N_8Cu_2F_{12}P_4$ requires C, 50.3; H, 3.9; N, 8.7%. δ_H (CD_3CN) 8.60 (4 H, s, $2 \times C_4H_2N_2$), 7.64 (4 H, s, $4 \times HC{=}N$), 7.34 (6 H, tr, J 7.5, $6 \times C_6H_5$), 7.20 (12 H, tr, J 7.5, $6 \times C_6H_5$), 6.84 (12 H, tr, J 8.5, $6 \times C_6H_5$), 4.31 (8 H, br mult, $4 \times {=}NCH_2$), 2.44 (2 H, br d, J 13.5, CCH_2C), and 2.44 (2 H, br mult, CCH_2C). δ_C (CD_3CN) 157, 153, 133 (d, J^2_{CP} 14), 132 (d, J^1_{CP} 31), 130, 129.1 (d, J^3_{CP}

9), 128.8, 63, 34. δ_P (CD_3CN) 0.76 (2 P, br s, 2 × PPh_3), −143.2 (2 P, sept, J_{PF} 707, 2 × PF_6). IR (KBr disk, inter alia) 3542 (sh), 3473 (sh), 3415 (s), 2922 (w), 1634 (w), 1617 (w), 1480 (w), 1440 (w), 1095 (w), 842 (s), 698 (m), 558 (s), 523 (m), 513 (m) cm^{-1}. λ(MeCN) = 246 sh ($\varepsilon = 44500$ l mol^{-1} cm^{-1}), $\lambda_{max} = 419$ nm ($\varepsilon = 10300$ l mol^{-1} cm^{-1}). Mass spectrum m/z 674 $[Cu_2(L1)(PPh_3)PF_6]^+$, 736 $[Cu_2(L1)(PPh_3)]^+$, 671 $[Cu(L1)(PPh_3)]^+$, 619 $[Cu_2(L1)PF_6]^+$, 474 $[Cu_2(L1)]^+$.

4.4. X-ray crystallography

Data were collected on a Siemens P4 four-circle diffractometer for **2** and **7**, and on a Bruker SMART diffractometer for **9** and **12**, using graphite-monochromated Mo–Kα radiation ($\lambda = 0.71013$ Å). The data were corrected for Lorentz and polarisation effects and empirical absorption corrections were applied. In **2**, **7** and **9** the structures were solved by direct methods whereas for **12** the structure was solved by Patterson methods (SHELXS-86 [19]), which, in each case, revealed most of the non-hydrogen atoms, and the remaining atoms were located from difference Fourier maps. Hydrogen atoms were inserted at calculated positions except where noted otherwise, and rode on the atoms to which they are attached (including isotropic thermal parameters which were equal to 1.2 times the equivalent isotropic displacement parameter for the attached non-hydrogen atom). The function minimised in the refinements was $\{\Sigma [w(F_o^2 - F_c^2)^2]/\Sigma [w(F_o^2)^2]\}^{1/2}$ where $w = [\sigma^2(F_o^2) + (aP)^2 + bP]^{-1}$ and $P = [2F_c^2 + \mathrm{Max}(F_o^2, 0)]/3$.

4.4.1. Crystal data for *[Cu$_2$(L1)Cl$_2$(H$_2$O)](ClO$_4$)$_2$ (2)•H$_2$O*

$C_{18}H_{24}Cl_4Cu_2N_{10}O_8$, brown triangular block, crystal dimensions 0.10 × 0.03 × 0.85 mm, orthorhombic space group *Cmc*2(1), $a = 24.24(2)$, $b = 10.177(4)$, $c = 10.394(3)$ Å, $U = 2564(3)$ Å^3, $Z = 4$, $\mu = 2.144$ mm^{-1}. 908 reflections were collected in the range $4 < 2\theta < 45°$ and the 908 independent reflections were used in the structural analysis. The structure was refined against all F^2 data (SHELXL-93 [20]). The refinement of 99 parameters (Cu and Cl atoms anisotropic) converged to $R_1 = 0.1363$ [for 568 reflections having $F > 4\sigma(F)$], $wR_2 = 0.5047$ and goodness of fit = 1.195 (for all 908 F^2 data).

4.4.2. Crystal data for *[Cu$_2$(L1)(H$_2$O)$_2$](ClO$_4$)$_4$ (7)*

$C_{18}H_{24}Cl_4Cu_2N_8O_{18}$, brown block, crystal dimensions 0.32 × 0.22 × 0.12 mm, monoclinic space group $P2_1/c$, $a = 9.415(3)$, $b = 8.979(4)$, $c = 18.562(6)$ Å, $\beta = 102.590(10)°$, $U = 1531.4(10)$ Å^3, $Z = 2$, $\mu = 1.833$ mm^{-1}, $T = 150$ K. 3069 reflections were collected in the range $4 < 2\theta < 45°$ and the 1994 independent reflections were used in the structural analysis. The structure was refined against all F^2 data (SHELXL-93 [20]). The refinement of 181 parameters (Cu, Cl, O and N atoms anisotropic, H atoms on the water molecule were located from difference maps then fixed) converged to $R_1 = 0.069$ [for 1207 reflections having $F > 4\sigma(F)$], $wR_2 = 0.131$ and goodness of fit = 1.06 (for all 1994 F^2 data).

*4.4.3. Crystal data for [$Cu^{II}Cu^{I}$(L1)$(NCS)_4$Cu]MeCN (**9**)*

$C_{24}H_{23}N_{13}Cu_3S_4$, brown block, crystal dimensions $0.74 \times 0.40 \times 0.28$ mm^3, triclinic space group $P\bar{1}$, $a = 6.6348(16)$, $b = 13.406(3)$, $c = 18.129(4)$ Å, $\alpha = 76.943(3)°$, $\beta = 81.886(3)°$, $\gamma = 80.918(3)°$, $U = 1541.8(6)$ Å^3, $\mu = 2.363$ mm^{-1}, $Z = 2$, $D_{calc} = 1.750$ Mg m^{-3}, $F(000) = 818$, $T = 168(2)$ K. 19868 reflections were collected in the range $4 < 2\theta < 50°$. A semi empirical absorption correction (SADABS) was applied ($T_{min} = 0.71$, $T_{max} = 1.00$) and the 6259 independent reflections used in the structural analysis. All non-hydrogen atoms were made anisotropic and the refinement (SHELXL-97) [20] of 398 parameters converged to $R1 = 0.0284$ [for 6259 reflections having $F > 4\sigma(F)$], $wR_2 = 0.0723$ and goodness of fit 1.052 (for all 6259 F^2 data). Peak/hole $0.531/-0.530$ e Å^{-3}.

*4.4.4. Crystal data for [Cu^{I}_2(L1)$(PPh_3)_2$]$(PF_6)_2$ (**12**)*

$C_{54}H_{50}N_8F_{12}Cu_2P_4$, deep red plate, crystal dimensions $0.71 \times 0.53 \times 0.03$ mm^3, monoclinic space group $P2_1/n$, $a = 15.173(5)$, $b = 10.704(4)$, $c = 17.536(6)$ Å, $\beta = 109.663(5)°$, $U = 2682.2(16)$ Å^3, $\mu = 1.001$ mm^{-1}, $Z = 2$, $D_{calc} = 1.597$ Mg m^{-3}, $F(000) = 1312$, $T = 163(2)$ K. 33875 reflections were collected in the range $4 < 2\theta < 53°$. A semi empirical absorption correction (SADABS) was applied ($T_{min} = 0.87$, $T_{max} = 1.00$) and the 5471 independent reflections used in the structural analysis. All non-hydrogen atoms were made anisotropic and the refinement (SHELXL-97) [20] of 370 parameters converged to $R_1 = 0.0323$ [for 3895 reflections having $F > 4\sigma(F)$], $wR_2 = 0.0849$ and goodness of fit 0.991 (for all 5471 F^2 data). Peak/hole $0.377/-0.323$ e Å^{-3}.

5. Supplementary material

Atomic coordinates, thermal parameters, and bond lengths and angles have been deposited at the Cambridge Crystallographic Data Centre, numbers CCDC 145496–145499 for compounds **2**, **7**, **9** and **12**. Copies of this information may be obtained free of charge form The Director, CCDC, 12 Union Road, Cambridge, CB2 1EZ, UK (fax: +44-1223-336033; e-mail: deposit@ccdc.cam.ac.uk or www: http://www.ccdc.cam.ac.uk).

Acknowledgements

We are grateful to B.M. Clark (University of Canterbury) for the FAB mass spectra, to Professor W.T. Robinson and Dr J. Wikaira (University of Canterbury) for the X-ray data collections, to N. Duffy (University of Otago) for helpful discussions and to M. Derrett, M. Pahl, W. Redmond (University of Otago) for their help. This research was supported in part by Public Good Science funding from the Foundation for Research, Science and Technology and the Marsden Fund, and by grants from the University of Otago and the Australian Research Council. SB thanks the University of Otago for the granting of study leave which

allowed the spectroelectrochemical and EPR measurements to be carried out, and gratefully acknowledges her host Professor K. Wieghardt and the financial support of the Alexander von Humboldt Stiftung. SB is grateful for the award of a Bilateral Research Activities Programme Grant (International Science and Technology Linkages Fund) which enabled her to visit KSM. DKK thanks Athabasca University for granting study leave and financial support.

References

[1] P.J. Steel, Coord. Chem. Rev. 106 (1990) 227.
[2] See for example: (a) L.K. Thompson, V.T. Chacko, J.A. Elvidge, A.B.P. Lever, R.V. Parish, Can. J. Chem. 47 (1969) 4141. (b) L.K. Thompson, A.W. Hanson, S.K. Mandal, J. Chem. Soc., Chem. Commun. (1985) 1709. (c) T.C. Woon, R. McDonald, S.K. Mandal, L.K. Thompson, S.P. Connors, A.W. Addison, J. Chem. Soc., Dalton Trans. (1986) 2381. (d) L.K. Thompson, S.K. Mandal, E.J. Gabe, F.L. Lee, A.W. Addison, Inorg. Chem. 26 (1987) 657. (e) L.K. Thompson, E.J. Gabe, F.L. Lee, Inorg. Chem. 27 (1988) 39. (f) S.K. Mandal, L.K. Thompson, E.J. Gabe, J.P. Charland, F.L. Lee, Inorg. Chem. 27 (1988) 855. (g) L.K. Thompson, S.S. Tandon, R.C. Hynes, Inorg. Chem. 31 (1992) 2210. (h) S.S. Tandon, L.K. Thompson, M.E. Manuel, J.N. Bridson, Inorg. Chem. 33 (1994) 5555.
[3] (a) F.W. Hartstock, L.K. Thompson, Inorg. Chim. Acta 72 (1983) 227. (b) S.K. Mandal, L.K. Thompson, E.J. Gabe, F.L. Lee, J.P. Charland, Inorg. Chem. 26 (1987) 2384. (c) L. Chen, L.K. Thompson, J.N. Bridson, Inorg. Chim. Acta 214 (1993) 67 (d) M. Maekawa, M. Munakata, T. Kuroda-Sowa, Y. Nozaka, J. Chem. Soc., Dalton Trans. (1994) 603.
[4] F. Abraham, M. Lagrenee, S. Sueur, B. Mernari, C. Bremard, J. Chem. Soc., Dalton Trans. (1991) 1443.
[5] S. Brooker, S.J. Hay, P.G. Plieger, Angew. Chem. Int. Ed. 39 (2000) 1968.
[6] (a) M.T. Youinou, N. Rahmouni, J. Fischer, J.A. Osborn, Angew. Chem. Int. Ed. Engl. 31 (1992) 733. (b) P. Hubberstey, C.E. Russell, J. Chem. Soc., Chem. Commun. (1995) 959. (d) P.N.W. Baxter, H. Sleiman, J.M. Lehn, K. Rissanen, Angew. Chem. Int. Ed. Engl. 36 (1997) 1294.
[7] (a) S. Brooker, R.J. Kelly, G.M. Sheldrick, J. Chem. Soc. Chem. Commun. (1994) 487. (b) S. Brooker, R.J. Kelly, J. Chem. Soc., Dalton Trans. (1996) 2117.
[8] S. Brooker, R.J. Kelly, B. Moubaraki, K.S. Murray, Chem. Commun. (1996) 2579.
[9] (a) S. Brooker, R.J. Kelly, P.G. Plieger, Chem. Commun. (1998) 1079. (b) S. Brooker, P.G. Plieger, B. Moubaraki, K.S. Murray, Angew. Chem. Int. Ed., 38 (1999) 408. (c) S. Brooker, R.J. Kelly, P.G. Plieger, unpublished results.
[10] See for example: (a) S.S. Tandon, L.K. Thompson, J.N. Bridson, Inorg. Chem. 32 (1993) 32. (b) L. Chen, L.K. Thompson, J.N. Bridson, Can. J. Chem. 71 (1993) 1086. (c) L. Chen, L.K. Thompson, S.S. Tandon, J.N. Bridson, Inorg. Chem. 32, (1993) 4063. (d) S.S. Tandon, L.K. Thompson, J.N. Bridson, M. Bubenik, Inorg. Chem. 32 (1993) 4621; and references therein.
[11] See for example: (a) R. Robson, Aust. J. Chem. 23 (1970) 2225. (b) B.F. Hoskins, N.J. McLeod, H.A. Schaap, Aust. J. Chem. 29 (1976) 515. (c) H. Okawa, S. Kida, Bull. Chem. Soc., Jpn. 45 (1972) 1759.
[12] See for example: (a) A.W. Addison, Inorg. Nucl. Chem. Lett. 12 (1976) 899. (b) R.C. Long, D.N. Hendrickson, J. Am. Chem. Soc. 105 (1983) 1513. (c) K. Nag, S.K. Mandal, B. Adhikary, J. Chem. Soc., Dalton Trans. (1986) 1175. (d) P. Lacroix, O. Kahn, F. Theobald, J. Leroy, C. Wakselman, Inorg. Chim. Acta, 142 (1988) 129. (e) S.S. Tandon, L.K. Thompson, J.N. Bridson, V. McKee, A.J. Downard, Inorg. Chem. 31 (1992) 4635.
[13] See for example: (a) R.R. Gagné, C.A. Koval, T.J. Smith, M.C. Cimolino, J. Am. Chem. Soc. 101 (1979) 4571. (b) R.R. Gagné, L.M. Henling, T.J. Kistenmacher, Inorg. Chem. 19 (1980) 1226. (c) L.K. Thompson, S.K. Mandal, E.J. Gabe, M.J. Newlands, Inorg. Chem. 28 (1989) 3707.

[14] M. Kumar, V.J. Aran, P. Navarro, A. Ramos-Gallardo, A. Vegas, Tetrahedron Lett. 35 (1994) 5723.
[15] B. Bleaney, K.D. Bowers, Proc. R. Soc. London A214 (1952) 451.
[16] (a) Z. Xu, L.K. Thompson, D.O. Miller, Inorg. Chem. 36 (1997) 3985. (b) L.K. Thompson, Z. Xu, A.E. Goeta, J.A.K. Howard, H.J. Clase, D.O. Miller, 37 (1998) 3217.
[17] J. Heinze, Angew. Chem. Int. Ed. Engl. 23 (1984) 831.
[18] W.J. Geary, Coord. Chem. Rev. 7 (1971) 81.
[19] G.M. Sheldrick, Acta. Cryst. Sect. A 46 (1990) 467.
[20] (a) G.M. Sheldrick, Methods Enzymol. 276 (1997) 628. (b) G.M. Sheldrick, T.R. Schneider, Methods Enzymol. 277 (1997) 319.